KONA Powder and Particle Journal

KONA Powder and Particle Journal No. 43 (2026) 3–21/https://doi.org/10.14356/kona.2026015 Review Paper

Discrete Particle Modeling and Simulation of Granular Flow —Pioneering Development of Numerical Prediction of Granular Flow and Fluid–Solid Multiphase Flow—†

Toshitsugu Tanaka [1,2]*, Toshihiro Kawaguchi [3], Takuya Tsuji [1] and Kimiaki Washino [1]

[1] *Department of Mechanical Engineering, Graduate School of Engineering, The University of Osaka, Japan*
[2] *Department of Mechanical Engineering, Faculty of Science and Engineering, Otemon Gakuin University, Japan*
[3] *Faculty of Societal Safety Sciences, Kansai University, Japan*

Discrete Element Method (DEM) was proposed by Cundall and Strack (1979) and gained traction in the field of powder engineering during the late 1980s. In the 1990s, various applications of DEM were conducted in the powder technology field, and the capability of DEM for predicting powder behavior was acknowledged. In the 2000s and 2010s, advancements in computing technology and the availability of general-purpose software led to the widespread adoption of numerical simulation as a prevalent tool in industrial applications. The authors have been engaged in discrete particle modeling of gas–solid two-phase flows and the development of DEM–CFD models for the numerical analysis of both dense gas–solid two-phase flows and gas–liquid–solid three-phase flows. Thus, this paper aims to provide a comprehensive description of the pioneering development of discrete particle models and simulations conducted by the authors.

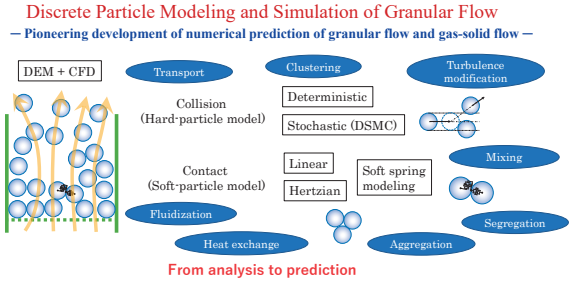

Keywords: discrete particle simulation, discrete element method, DEM–CFD simulation, modeling for DEM simulation, applications of DEM

1. Introduction

The authors have been engaged in the modeling and numerical simulation of gas–solid two-phase flows as well as gas–liquid–solid three-phase flows in the presence of particle interactions. This review presents the authors' contributions to the development of numerical models and simulations.

The numerical models for granular materials are classified into two categories: discrete particle models and continuum models (see **Section 2.2** for a detailed description). The authors have made pioneering contributions to discrete particle modeling and simulations involving particle interactions. In the field of gas–solid flows, until the mid-1980s, there had been few studies of particle collisions in numerical simulations using discrete particle models for relatively dilute gas–solid two-phase flows, such as low concentration fast transport in pneumatic conveying. Subsequently, Tanaka et al. (1990) and Tanaka and Tsuji (1991) proposed a methodology for the identification and incorporation of particle–particle collisions within numerical simulations to facilitate a more profound comprehension and elucidation of the dynamics of particle motion within a vertical pipe, as well as to reproduce the particle velocity and concentration distributions measured in their experiments (Tanaka et al., 1989). Subsequently, the proposed methodology was applied to a diverse array of flows.

Discrete Element Method (DEM) (Cundall and Strack, 1979) was successfully applied to the numerical simulation of plug flow in a horizontal pipe (Tanaka et al., 1991a; Tsuji et al., 1992), where the particle–particle interaction cannot be modeled by particle collisions. Subsequently, the DEM–CFD method was proposed as a means to simulate the fluidized behavior of a two-dimensional gas-fluidized bed (Kawaguchi et al., 1992; Tanaka et al., 1993; Tsuji et al., 1993). The proposed method allowed the numerical prediction of general dense gas–solid two-phase flows as well as gas–liquid–solid three-phase flows and was subsequently extended to various broad applications.

DEM, first proposed in 1979, gained traction in the field of powder engineering during the late 1980s. In the 1990s, various applications of DEM were conducted in the powder technology field, and the capability of DEM for predicting powder behavior was acknowledged. In subsequent decades, namely, the 2000s and 2010s, advancements in computing technology and the widespread availability of

† Received 31 March 2025; Accepted 4 June 2025
J-STAGE Advance published online 29 July 2025
* Corresponding author: Toshitsugu Tanaka;
[1] Add: 2-1, Yamada-oka, Suita, Osaka 565-0871, Japan
[2] Add: 2-1-15 Nishiai, Ibaraki, Osaka 567-8502, Japan
E-mail: to-tanaka@otemon.ac.jp
TEL: +81-72-641-9157

general-purpose software led to the broad adoption of numerical simulation as a standard tool in industrial applications.

The DEM is a numerical method that tracks the motion of individual particles. It is classified as a discrete particle model in which particle–particle interactions are represented by contact forces. The proposed method is often considered universally applicable because it covers a wide range of particle interactions, from collisions to contact. However, depending on the target powder/particle behavior, the particle–particle interactions within it may be dominated by collisions or persistent contact, and the conditions required for the DEM contact force model are different in each case.

This article reviews the development of discrete particle models and simulation methods for granular flow prediction, which were carried out by the authors. This review is intended to support future developments in DEM modeling and simulation methods.

2. Model classification

In this chapter, a classification of mathematical models of fluid–solid multiphase flows is presented. **Section 2.1** proposes a classification of models for granular media based on the spatial resolution relative to the particle scale. These models are divided into two categories: discrete particle models and continuum models. In contrast, **Section 2.2** focuses on models for fluid media, which are categorized into two types: locally averaged flow models and particle-resolved flow models. The discrete particle models are further classified into two distinct types: collision models and contact models. The collision model assumes that a particle is modeled as a hard particle that interacts with another particle through collisions, whereas the contact model assumes that a particle is modeled as an elastic particle that interacts with other particles through contacts.

2.1 Continuum and discrete particle models

As illustrated in **Fig. 1**, mathematical models of solid and fluid phases can be classified based on their spatial resolution. These models are primarily divided into two categories: macroscopic and microscopic. The microscopic category includes discrete particle models that focus on and track the motion of individual particles from a microscopic perspective. In contrast, the continuum model represents a group of particles as a continuum from a macroscopic perspective in comparison to the scale of individual particles. With regard to the fluid phase, the microscopic flow model is the one that satisfies the non-slip boundary condition at the surface of individual particles and resolves the flow between particles, namely, Direct Numerical Simulation (DNS) or particle-resolved simulation. In contrast, the local mean flow model deals with the flow field of a fluid that is locally volume-averaged on a scale larger than the particle size. The characteristics of each model are illustrated in **Fig. 1**. The basic equations for the two-fluid model, which couples the continuum model for the granular medium with the locally averaged flow model for the fluid medium, were derived by Anderson and Jackson (1967).

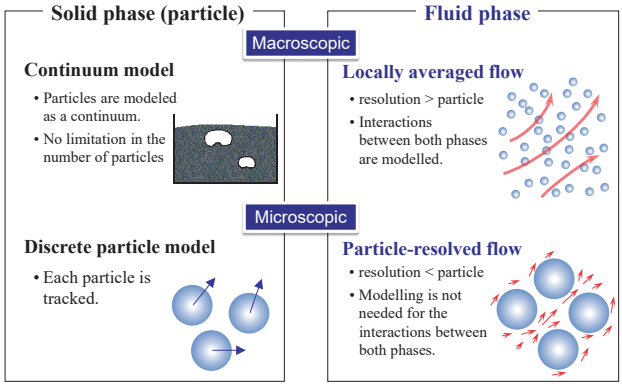

Fig. 1 Classification of numerical models for solid and fluid phase.

The discrete particle model can be coupled with either locally averaged or particle-resolved flow of the fluid phase. In some cases, the effects such as liquid bridge or lubrication—arising from the presence of liquid in narrow gaps between particles—are not directly resolved, but are modeled even in particle-resolved simulations.

With regard to particle models, discrete particle models hold significant value due to their ability to straightforwardly introduce the influence of various factors at the particle motion level. These factors include size distribution, particle shape, adhesion, liquid addition, and lubrication. This feature enables the direct determination of phenomena, such as particle mixing, diffusion, and segregation, without the necessity for additional models. However, it should be noted that as the number of particles handled increases, the computational load also increases. In contrast, the continuum model has the advantage that the computational load is not dependent on the number of particles. However, the advantages of the discrete particle model described above are lost in the continuum approach.

2.2 Collision model vs. contact model

Discrete particle models are generally classified into two categories: rigid and elastic particle models, as illustrated in **Fig. 2**. In rigid particle models, particle–particle or particle-wall interactions are modeled as collisions. Conversely, in elastic particle models, these interactions are modeled as contacts. The rigid particle model can be regarded as a collision model, whereas the elastic particle model can be considered a contact model. The rigid particle model disregards the time required for collisions and does not account for many-body collisions. In contrast, elastic particle models represent collisions by momentum exchange due to contact forces for a finite time and can represent

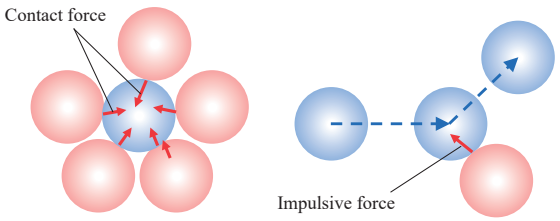

Fig. 2 Classification of discrete-particle models from the viewpoint of particle–particle interaction.

many-body collisions and persistent contact. The particle models used in the discrete element method are classified as elastic particle models.

3. Development in collision model

This chapter is devoted to presenting the development of numerical methods and simulations in intermediate concentration flows where the particle–particle collision plays an important role in the behavior of particles.

In the late 1980s, the challenge of numerical simulation of gas–solid two-phase flows began (Crowe, 1982; Crowe et al., 1977; Tsuji et al., 1987b). The advent of discrete particle simulations with two-way coupling of dilute gas–solid two-phase flows can be traced back to the Particle-Source-In Cell (PSI Cell) model pioneered by Crowe et al. (1977). The PSI Cell model maps the momentum exchange between the particle and fluid to the fluid computational cell containing the particle, thereby allowing a two-way calculation that takes into account the interaction between the two phases.

Tsuji et al. (1987a, b) performed discrete particle simulations of gas–solid two-phase flows in a horizontal channel (Tsuji et al., 1987b) and a gas–solid two-phase jet (Tsuji et al., 1987a). They assumed massive particles for which diffusion is not controlled by fluid turbulence because of their large inertia. The irregular bouncing model proposed by Tsuji et al. (1987b) for flow in a horizontal channel aimed to maintain particle suspension; however, it could not qualitatively reproduce the distributions of particle velocity and concentration measured in a horizontal pipe by Morikawa et al. (1985). Although they pointed out the possibility of the effects of particle–particle collisions, there were few discrete particle simulations with particle–particle collisions at the time. The majority of research interest in discrete particle simulations at that time focused on the interaction between gas turbulence and particles (Gore and Crowe, 1989; Hetsroni, 1989).

3.1 Deterministic method

In their seminal work (Tanaka et al., 1990; Tanaka and Tsuji, 1991), Tanaka and colleagues pioneered a discrete particle simulation of gas–solid two-phase flow with particle–particle collisions in a vertical pipe. In this groundbreaking study, the deterministic method was employed to treat particle–particle collisions, marking a significant advancement in the field. The equations of motion for individual particles were numerically integrated at each time step to update the position, velocity, and angular velocity. To ensure the accuracy of the simulation, the time step, Δt, must be set sufficiently small compared to the mean free time for particle–particle collisions. The occurrence of a particle–particle collision is detected based on the intersection of the trajectories of the relative motions of the individual particles during the time progression of Δt. In the event of a collision, the velocity and subsequent angular velocity are determined based on the equation of motion for impact. The position of the collision is determined by accounting for the change in trajectory resulting from the collision.

The employment of this deterministic method results in an increase in computational time for detecting particle–particle collisions that is proportional to the square of the number of particles, in the absence of appropriate computational load reduction methods. To address this issue, the cell registration method was employed, which involved dividing the calculation domain into smaller cubic cells, where each cell was smaller than the mean free path of the particles. In this method, each particle in the simulation is assigned to a cell in which it is contained. The detection of colliding particles is not applied to all particle combinations; rather, it is applied to the particles in neighboring cells. Prior to the proposal of this method, no well-defined method was available for calculating particle collisions, and this method remains a widely used approach. The particle velocity and concentration distributions for gas–solid two-phase flow in a vertical pipe calculated using the deterministic method are shown in **Fig. 3**. As the particle concentration increases, the particle concentration distribution becomes more uniform because of the particle diffusion caused by inter-particle collisions, and the results are consistent with the experimental observations.

Subsequently, deterministic calculations of particle–particle collisions were employed to investigate the impact of particle collisions in gas–solid two-phase turbulence in vertical channels (Yamamoto et al., 2001) (**Fig. 4**) and in rotating turbulent channel flows (Pan et al., 2000, 2001, 2002). Additionally, the formation of clusters in gas–solid two-phase flows with intermediate concentrations observed in the riser of a circulating fluidized bed (Tsuji et al., 2008a) was also investigated (**Fig. 5**).

3.2 Stochastic method

The deterministic method is accurate; however, it requires a significant amount of computational time to determine whether each particle collides with all of its possible neighbors. Stochastic methods are available to reduce this

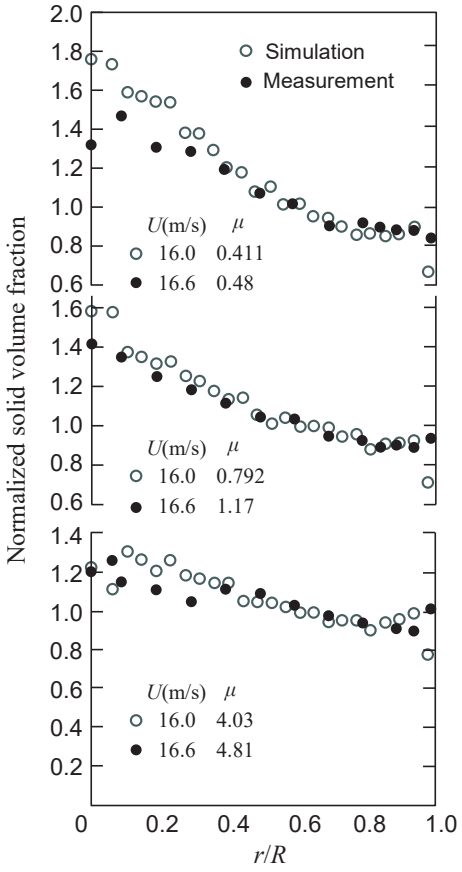

Fig. 3 Particle concentration distribution was predicted using the deterministic method (comparison with experiment) (Tanaka and Tsuji, 1991).

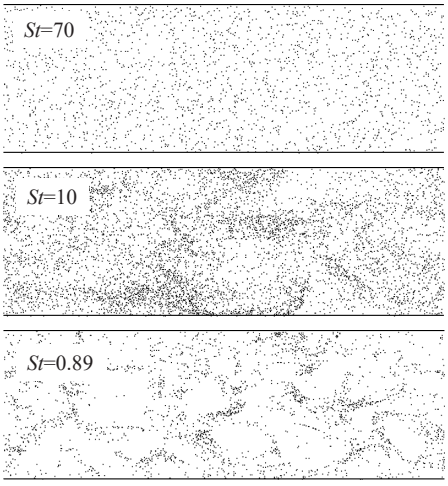

Fig. 4 Effect of Stokes number on the instantaneous particle distribution in the gas–solid turbulent flow in vertical channel. Reprinted from Ref. (Yamamoto et al., 2001). Copyright (2001), with permission from Cambridge University Press.

computational burden. As a probabilistic method, we proposed applying the Direct Simulation Monte Carlo method (DSMC method), which is used to calculate the molecular motion of dilute gases (Bird, 1994; Nanbu, 1980), to particle–particle collisions. The collision probability of a molecule can be given by the velocity distribution function in the vicinity of the molecule. The Monte Carlo method, which involves calculating the collision probability based on the velocity distribution function of the sample molecules assuming the number density of molecules in the population and performing a random dice roll based on this probability, is employed to determine whether there is a collision and to identify the collision pair.

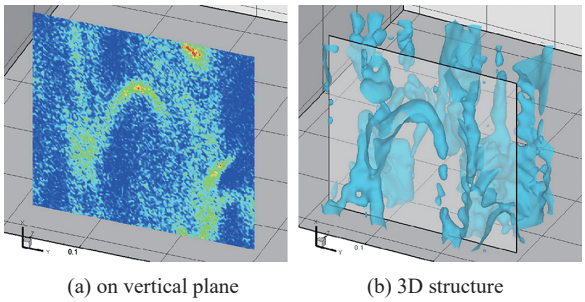

Fig. 5 3D structure of particle clusters. Reprinted from Ref. (Tsuji et al., 2008a). Copyright (2008), with permission from Elsevier.

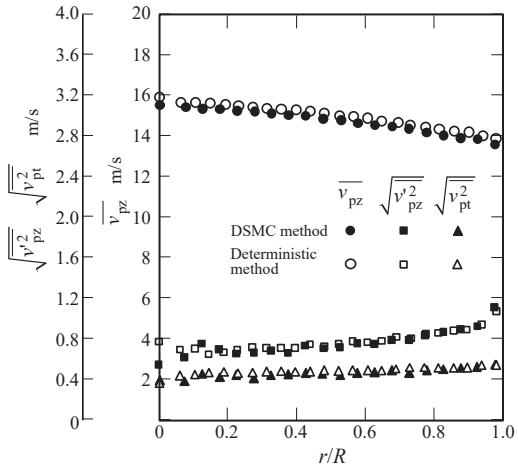

Fig. 6 Comparison between the results of the deterministic and DSMC methods (Tanaka et al., 1991b). $\overline{v_{pz}}$: average particle velocity in the vertical direction, $\sqrt{v_{pz}^2}$, $\sqrt{v_{pt}^2}$: fluctuation particle velocities in the vertical and transverse directions, respectively.

The DSMC method was demonstrated to be effective for representing the flow within a vertical pipe, as illustrated in **Fig. 6** (Tanaka et al., 1991b). This method has also been shown to be capable of predicting cluster formation in the riser of a circulating fluidized bed (Tanaka et al., 1995, 1996).

4. Contact force model of the DEM

The contact force model of the DEM, a typical elastic particle model, is depicted in **Fig. 7**. The model can be broadly classified into two categories: (1) a linear model that employs linear springs and dashpots, and (2) a nonlinear model that uses a theoretical solution based on the contact theory of isotropic elastic bodies. According to Hertz's contact theory (Johnson, 1985), the normal elastic

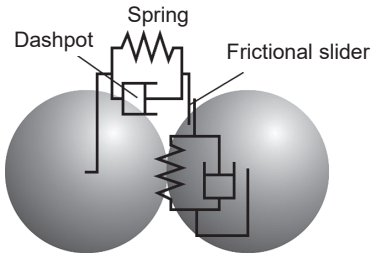

Fig. 7 Contact force model of Discrete Element Method.

repulsive force f_{Cn} of two spherical particles is given by

$$f_{Cn} = \kappa_n \delta_n^{\frac{3}{2}} \tag{1}$$

$$\kappa_n = \frac{\sqrt{2a}E}{3(1-\sigma^2)} \tag{2}$$

where, in the context of spherical particles of uniform material and diameter, a is the particle radius, δ_n, the normal deformation, E, the Young's modulus, and σ, the Poisson's ratio. As illustrated in **Eqn. (1)**, the relationship between the elastic repulsive force, f_{Cn}, and the deformation, δ_n, of the spherical particles is not linear.

DEM was employed to reproduce the behavior of a plug in a horizontal pipe numerically (Tanaka et al., 1991b; Tsuji et al., 1992). In the original DEM paper by Cundall and Strack, a linear model was used as the contact force model. However, the dependence of the phenomenon on the contact force model was not clear at the time, so a more physically rigorous Hertz-Mindlin model (Johnson, 1985; Mindlin, 1949; Mindlin and Deresiewicz, 1953) was used. The elastic repulsive force can be determined from the physical properties of the particles, such as Young's modulus and Poisson's ratio. A key issue is how to provide viscous damping by dashpots. The following model for viscous damping, which is entirely original, was constructed on the basis of theoretical considerations (Tanaka et al., 1991b; Tsuji et al., 1992):

$$f_{Vn} = \alpha\sqrt{m\kappa_n}\,\delta_n^{\frac{1}{4}}\dot{\delta}_n \tag{3}$$

The parameter α, which is a model parameter, has a relationship with the repulsion coefficient e, as illustrated in **Fig. 8**. In other words, the proposed model allows the repulsion coefficient of a particle to be set arbitrarily. The viscous damping force model defined by **Eqn. (3)** was developed not from the physics of the contact of elastic spheres but from the viewpoint of easy control of the repulsive properties of particles. This contact force model was employed in the simulation of plug flow in a horizontal pipe, and the results are presented in **Fig. 9**.

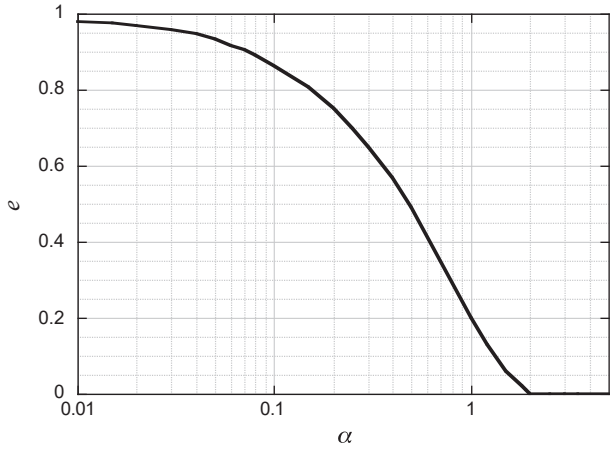

Fig. 8 Relationship between parameter α and restitution coefficient e. Reprinted from Ref. (Tsuji et al., 1992). Copyright (1992), with permission from Elsevier.

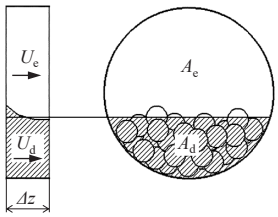

(a) DEM-pipe-flow coupling model

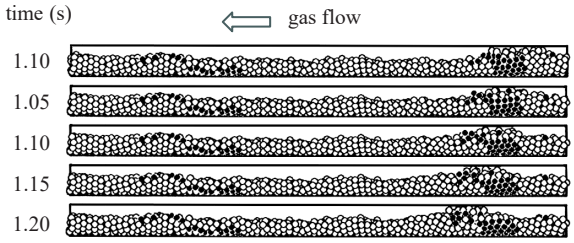

(b) Results

Fig. 9 DEM–Fluid coupling simulation of horizontal plug flow. Reprinted from Ref. (Tsuji et al., 1992). Copyright (1992), with permission from Elsevier.

5. DEM–CFD coupling model

5.1 Modeling horizontal plug flow

The study of plug flow in a horizontal pipe (Tanaka et al., 1991b; Tsuji et al., 1992) is the world's first numerical simulation to combine DEM and CFD. As shown in **Fig. 9(b)**, the plug flow in a horizontal pipe consists of a region in which the horizontal pipe is divided into (1) a particle-deposition layer at the bottom and an empty channel at the top, and (2) a plug region where the entire cross-section is filled with particles. The pipe was divided into small regions, as shown in **Fig. 9(a)**. The fluid flow and the fluid forces acting on the particles are obtained by a parallel channel model, which applies the Ergun equation (Ergun, 1952) to the particle-deposition layer and assumes the frictional resistance of the pipe in the empty channel section. The flow patterns obtained are in good agreement

with experimental results (Tsuji and Asano, 1990) in terms of the thickness of the particle-deposition layer and the movement velocity of the plug flow.

5.2 DEM–CFD coupling simulation of the fluidized bed

The fluid flow calculation and DEM coupling model described in **Section 5.1** are specific to the plug flow in a horizontal pipe. The DEM–CFD coupling model was developed to calculate the coupled flow of a fluid flow with a generalized group of highly concentrated particles (Kawaguchi et al., 1992; Tsuji et al., 1993). This allows the numerical prediction of the fluidized behavior of dense particles in a fluidized bed.

The fundamental equation for fluid flow was taken from the two-fluid model (TFM) proposed by Anderson and Jackson (1967) and applied to a spatial scale beyond the particle size by local volume averaging. The Ergun equation (Ergun, 1952) for the high-concentration region and the Wen-Yu equation (1966) for the moderately dense region were adopted as models for the momentum exchange between particles and fluid due to the fluid force. These equations were previously used in the two-fluid model for fluidized beds (Bouillard et al., 1989). The bubbling fluidization patterns obtained from the calculations were compared with those from the validation experiments, as shown in **Fig. 10**. The simulated bubbling fluidization patterns agreed well with the experimental results, including the bubble generation period and rise rate. The above simulation of bubble formation was performed under the central gas injection condition. As shown in **Fig. 11**, using the DEM–CFD coupling model, bubble formation under uniform gas injection conditions was predicted by Tanaka et al. (1993).

In the numerical simulation of fluidization behavior using the DEM–CFD coupling model presented here, a linear model was used as the contact force model between particles, and the spring constant was reduced to lower the computational load. This was investigated by Kawaguchi (2003), who found that the calculation results were largely unaffected by the contact force model and the spring constant with respect to the bubbling fluidized behavior. As described in Chapter 6, most non-cohesive particles in a fluidized state are subject to a collision-dominated flow in which they interact through collisions. Consequently, these particles are in a kinetic state that can be adequately represented by a rigid particle model. This implies that the calculation results are independent of the contact force model, provided that the collision characteristics, such as the restitution coefficient, remain constant.

The DEM–CFD model has been applied to a two-dimensional fluidized bed with inserted baffles (Kawaguchi et al., 1998), a two-dimensional pulsating fluidized bed (Miyoshi et al., 2000), density wave formation in dense gas–solid flows in a vertical pipe (Kawaguchi et al., 2000b), quasi-three-dimensional numerical simulation of spouted beds in a cylinder (Kawaguchi et al., 2000a) (**Fig. 12**), and a fluidized bed containing Geldart-A particles (Kobayashi et al., 2011). Gera et al. (1998) performed numerical simulations of fluidized beds using both DEM–CFD and TFM to compare the behavior of a single rising bubble. The results showed that DEM–CFD was more accurate than TFM in predicting bubble shape, rising velocity, and void distribution.

6. Modeling of DEM simulations

6.1 Dynamic adhesion force model

In **Section 5.2**, it was stated that particles in a fluidized state are in a collision-dominated flow state, with relatively little influence from contact force models and spring constant dependence. However, DEM–CFD simulations of a fluidized bed of small particles (Geldart-A particles), where the influence of adhesion due to van der Waals forces is evident, show that the calculated results are significantly dependent on the spring constant, as shown in **Fig. 13** (Kobayashi et al., 2013). In particular, the smaller the spring constant, the more pronounced the adhesion effect becomes.

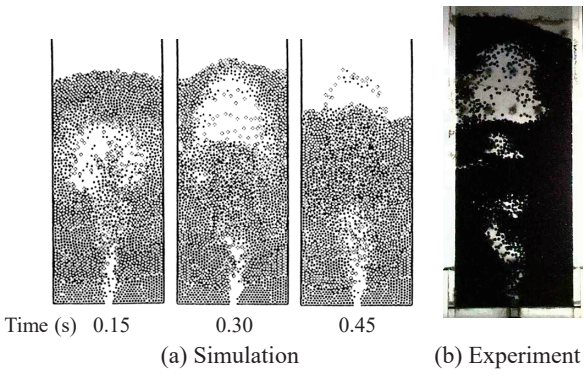

Fig. 10 Bubbling fluidized pattern simulated by DEM–CFD coupling model with the central gas injection. **(a)** is reprinted from (Tsuji et al., 1993). Copyright (1993), with permission from Elsevier, and **(b)** is reprinted from (Kawaguchi, 2003).

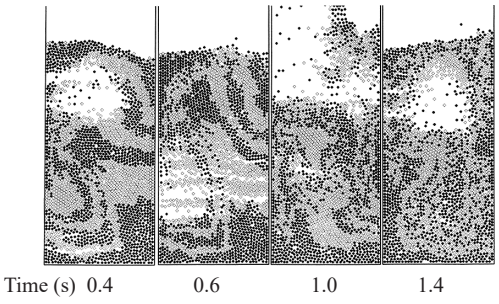

Fig. 11 Bubbling fluidized pattern simulated by DEM–CFD coupling model with uniform gas inflow. Reprinted from Ref. (Tanaka et al., 1993). Copyright (1993), with permission from World Scientific Publishing Co.

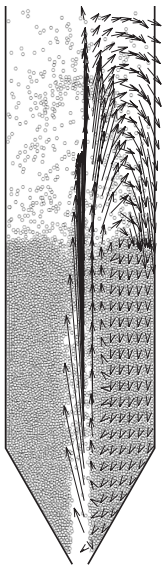

Fig. 12 Particle velocity distribution in the spouted bed predicted by the quasi-three-dimensional simulation. Reprinted from Ref. (Kawaguchi et al., 2000a). Copyright (2000), with permission from Elsevier.

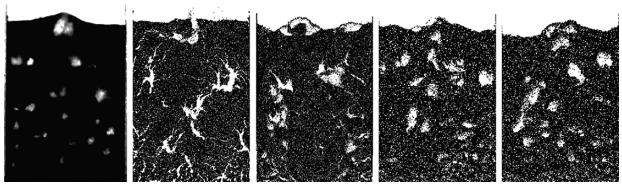

Fig. 13 Effect of spring constant on fluidized cohesive particle pattern. Reprinted from Ref. (Kobayashi et al., 2013). Copyright (2013), with permission from Elsevier.

Kobayashi et al. (2013) theoretically derived the dependence of the critical collision velocity, defined as the maximum collision velocity that exhibits adhesion without repulsion, on the spring constant. The function is given by the following equation:

$$v_c \propto \frac{F_{AD}}{\sqrt{mk}} \tag{4}$$

where, v_c is the critical collision velocity, F_{AD}, adhesion force, m, particle mass, and k, normal spring constant. Based on this relationship, they proposed the dynamic adhesion force model (DAFM), where the adhesion force used in the simulation is modified so as to keep the critical collision velocity constant according to the reduced spring constant used in the simulation.

Fig. 14 shows the relationship between the restitution coefficient and the collision velocity under the influence of the cohesion force (Tanaka et al., 2024). When the spring constant is reduced by a factor of 10^{-2} from the original condition without changing the adhesion force, the critical collision velocity is overestimated by a factor of 10. In contrast, the DAFM expressed the relationship well for the

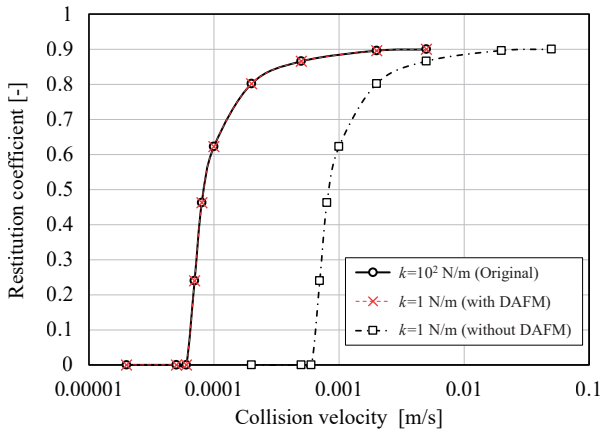

Fig. 14 Relationship between collision velocity and restitution coefficient. Reprinted from Ref. (Tanaka et al., 2024) under the terms of the CC BY-NC-ND 4.0 license.

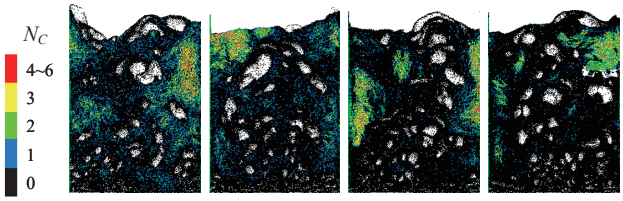

(a) k=10 N/m (b) k=100 N/m (c) k=1000 N/m (d) k=7000 N/m

Fig. 15 Fluidized pattern and coordination number distribution predicted by the dynamic adhesion force model. Reprinted from Ref. (Kobayashi et al., 2013). Copyright (2013), with permission from Elsevier.

original condition.

The predicted results of the bubbling fluidized behavior by using DAFM are shown in **Fig. 15** (Kobayashi et al., 2013). The color of the particle indicates the coordination number, which is the instantaneous number of particles in contact. The coordination number of most particles is zero, which indicates that inter-particle collision interactions dominate. A group of particles with a large coordination number forms an agglomerate. The figure shows that DAFM well expresses the effect of adhesion force on aggregation formation in the fluidized bed of Geldart-A particles.

From the above description in this section and the results shown in **Figs. 14** and **15**, it is clear that the DAFM can effectively represent the collision behavior of particles near the critical collision velocity. However, it is not clear whether the model can accurately represent the dynamics in the state where particle agglomeration has developed (i.e., contact-dominated flow). Therefore, to investigate the effectiveness of DAFM in contact-dominated flow, a numerical simulation of the simple shear flow of cohesive particles was performed (Tanaka T. et al., 2024).

Fig. 16 plots the relationship between the shear rate and shear stress obtained from the simulations. The simulations were performed using the Lees-Edwards shear period boundary in a two-dimensional calculation with a single

layer of particles. In the high shear-rate regime, the particle–particle interaction is collision-dominated, and the shear stress is proportional to the shear rate. In the low shear-rate region, all particles agglomerate to form large aggregates, and the particle–particle interaction is dominated by contact forces. As shown in the figure, the DAFM accurately represents the cohesive nature of the original system with respect to the fluid-to-solid phase transition of the granular medium due to a reduction in the shear rate, as well as the shear stress of the granular medium, except in the case of the maximum reduction in the spring constant.

Fig. 17 compares the time evolution of the granular structure under low shear-rate conditions. The DAFM accurately represented the time evolution of the granular structure under the original condition. The uniformly dispersed particles in the initial state gradually agglomerate and finally form a uniform large agglomerate. When the spring constant is reduced to $k_R = 1$ [N/m], and DAFM is not applied, a faster development of the agglomerate is predicted.

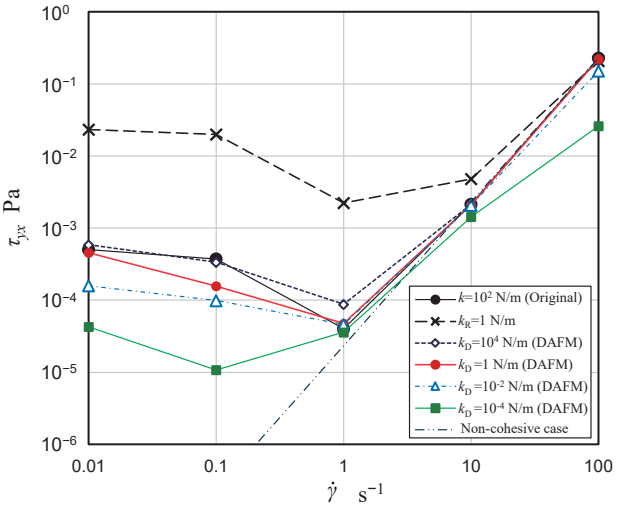

Fig. 16 Relationship between shear rate and shear stress in the shear flow of cohesive particles. Reprinted from Ref. (Tanaka et al., 2024) under the terms of the CC BY-NC-ND 4.0 license.

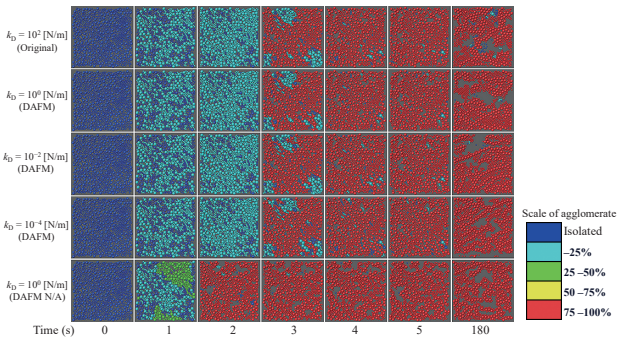

Fig. 17 Comparison of the time evolution of the granular structures ($\phi = 0.7$, $\dot{\gamma} = 0.01$ [s^{-1}]). The color of particle indicates the scale of the agglomerate, which is defined as the percentage of the total solid volume. Reprinted from Ref. (Tanaka et al., 2024) under the terms of the CC BY-NC-ND 4.0 license.

As shown in **Figs. 16** and **17**, the DAFM accurately captured the fully developed internal structures of the sheared particles and their temporal evolution. The availability of the DAFM in the contact-dominated regime (**Fig. 16**) cannot be explained by the critical collision velocity shown in **Fig. 14**. The bond-breaking model was proposed and used to provide a theoretical explanation of the applicability of the DAFM to the contact-dominated regime and the limit of the reduction rate of the spring constant.

6.2 Reduced Particle Stiffness (RPS) scaling of cohesive particles

The DAFM employs a linear model for the contact force calculation with the constant cohesion force so that the critical collision velocity can be theoretically derived. However, it is challenging to obtain the theoretical critical collision velocity when using nonlinear contact models or other types of cohesion forces, such as liquid bridge forces. This is because these forces are typically complex functions of particle position and velocity. Washino et al. (2018a) derived a more general cohesion force scaling: reduced particle stiffness (RPS) scaling. The RPS scaling is derived from the non-dimensionalized equation of motion of particles during binary collision, which ensures the invariance of the dimensionless cohesion force when the particle stiffness (i.e., spring constant or Young's modulus) is reduced. As shown in **Fig. 18**, the original coefficient of restitution was well reproduced by RPS scaling, i.e., (a) $F_{AO\_R}/F_{AO\_O} = 0.01$ and (b) $F_{AO\_R}/F_{AO\_O} = 0.00063$. It is noteworthy that the RPS scaling can be simplified to DAFM when a linear model with constant cohesion force is used.

Washino et al. (2024) further derived the scaling laws from general dimensionless equations of motion, which are for both particle translation and rotation, as well as multi-body interactions. In this way, they derived not only the cohesion force scaling but also the rolling resistance scaling. They also concluded that RPS scaling can properly capture the original particle behavior in Couette flows, but some discrepancies were observed when the particle stiffness was largely reduced. This may be because of the reduction of contact frequency.

6.3 Coarse grain model

One of the major problems of DEM is its extremely high computational cost when tracking many particles. Even with the recent advancement of computers, it is still practically impossible to complete the simulation of industrial-scale systems within an acceptable period. Coarse grain models are an increasingly popular method for reducing computational cost in DEM simulations: the particle size is artificially "scaled-up" while keeping the system size the

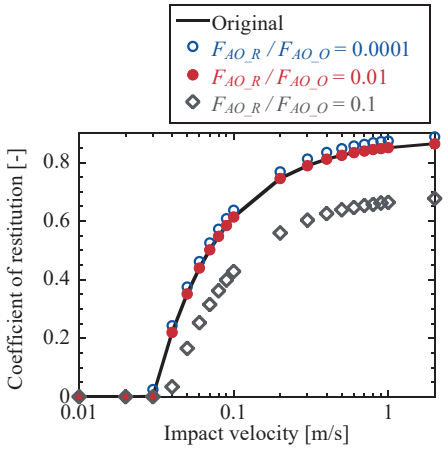

(a) Linear model with lubrication force

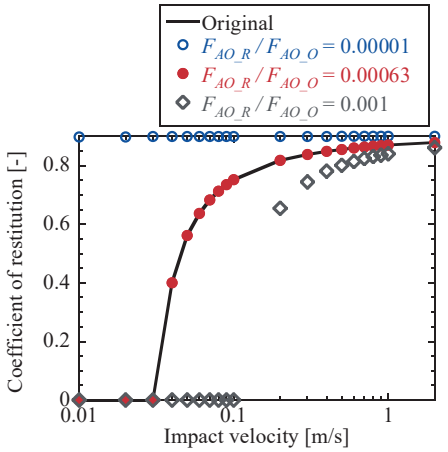

(b) Nonlinear model with linear cohesion force

Fig. 18 Relationship between net coefficient of restitution and impact velocity. Reprinted from Ref. (Washino et al., 2018a). Copyright (2018), with permission from Elsevier.

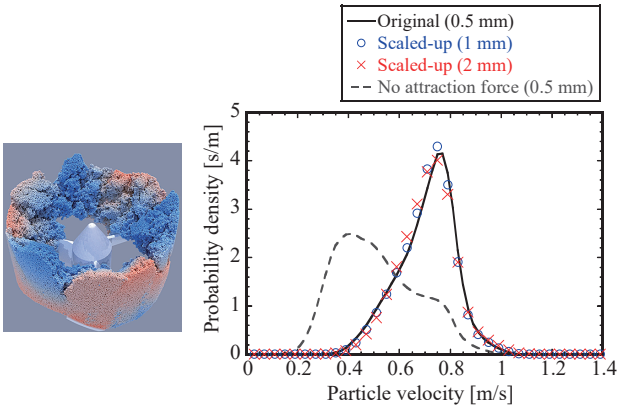

Fig. 19 Coarse-grained simulations of cohesive particles in a vertical mixer. Reprinted from Ref. (Hu et al., 2022), Copyright (2022), with permission from Elsevier.

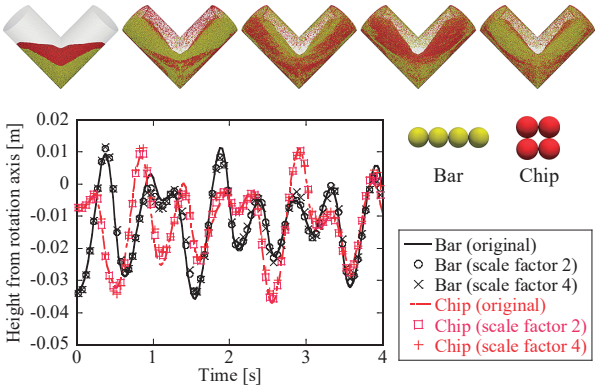

Fig. 20 Coarse-grained simulations of non-spherical particles in a V-mixer. Reprinted from Ref. (Washino et al., 2023a) under the terms of the CC BY-NC-ND 4.0 license.

same so that the total number of particles is reduced and the time step is increased. Chan and Washino (2018) classified coarse grain models in the literature into two categories parameter scaling and direct force scaling. In parameter scaling, the input parameters of the coarse-grained particles are adjusted to achieve similarity with the original particle system (Bierwisch et al., 2009; Jiang et al., 2020; Thakur et al., 2016). On the other hand, in direct force scaling, the forces acting on the original particles are first estimated using the original particle parameters and variables, which are then directly scaled up for the coarse-grained particles (Sakai et al., 2012; Sakai and Koshizuka, 2009).

Recently, the authors proposed a novel coarse-grain model with direct force scaling (Chan and Washino, 2018; Hu et al., 2022, 2024; Washino et al., 2021a, 2023a), which is called Scaled-Up Particle (SUP) model and based on a set of universal scaling laws to preserve the fluxes of momentum and angular momentum. It only requires two scaling laws for the forces, i.e., one for the inter-particle forces and the other for the body forces, together with one scaling law for inter-particle torques:

$$\boldsymbol{F}_{\mathrm{IS}} = l^2 \boldsymbol{F}_{\mathrm{IO}} \tag{5}$$

$$\boldsymbol{F}_{\mathrm{BS}} = l^3 \boldsymbol{F}_{\mathrm{BO}} \tag{6}$$

$$\boldsymbol{M}_{\mathrm{IS}} = l^2 \boldsymbol{M}_{\mathrm{IO}} \tag{7}$$

where l is the scale factor (i.e., the size ratio between the coarse grained and original particles), $\boldsymbol{F}_{\mathrm{I}}$ represents arbitrary inter-particle forces, $\boldsymbol{F}_{\mathrm{B}}$ arbitrary body forces and $\boldsymbol{M}_{\mathrm{I}}$ arbitrary inter-particle torques. The subscripts O and S indicate the original and coarse-grained systems, respectively. The SUP model can accurately replicate the original particle behavior in various systems, including cohesive (**Fig. 19**), non-spherical (**Fig. 20**), and poly-dispersed particles (**Fig. 21**), as well as gas–liquid–solid three-phase systems (**Fig. 22**).

6.4 Modeling for liquid bridge force

In many powder handling processes, including wet granulation and particle coating, liquid is often added and mixed with dry powder for various purposes. The formation of liquid bridges creates additional bonding forces between particles, namely capillary and viscous forces. It is well known that even a small amount of liquid can

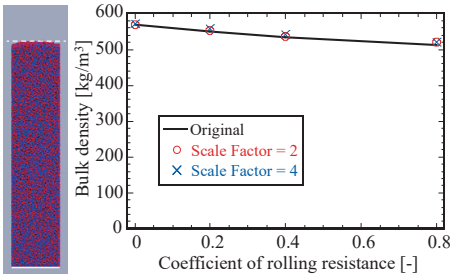

Fig. 21 Coarse-grained simulations of polydispersed particles with different coefficient of rolling resistance. Reprinted from Ref. (Hu et al., 2024). Copyright (2024), with permission from Elsevier.

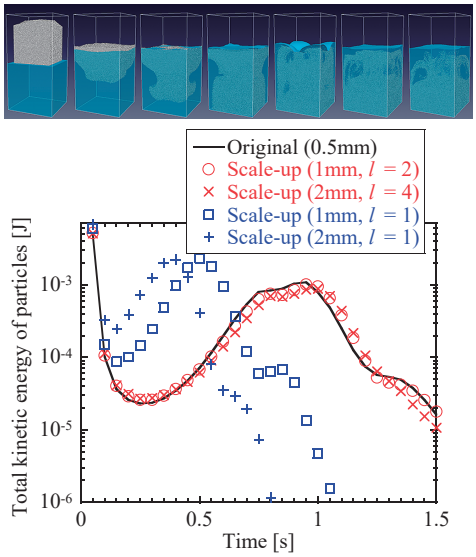

Fig. 22 Coarse-grained simulations of gas–liquid–solid three-phase flow. Reprinted from Ref. (Washino et al., 2021a). Copyright (2021), with permission from Elsevier.

significantly affect the powder flow behavior. Capillary forces arise from the sum of the surface tension along the three-phase contact line and the pressure difference across the meniscus (i.e., Laplace pressure). Many capillary force models have been proposed in the literature, and they are largely comparable (Lambert et al., 2008; Mikami et al., 1998; Muguruma et al., 2000; Rabinovich et al., 2005).

Viscous forces are caused by the relative movement between particles and liquid bridges and are often modeled using the Reynolds lubrication theory. The viscous forces, $\boldsymbol{F}_{\mathrm{vis}}$, can be written in the following generic form (Washino et al., 2016):

$$\boldsymbol{F}_{\mathrm{vis}}^{\mathrm{n}} = -C_{\mathrm{N}}\boldsymbol{v}_{\mathrm{rel}}^{\mathrm{n}} \tag{8}$$

$$\boldsymbol{F}_{\mathrm{vis}}^{\mathrm{t}} = -\left(C_{\mathrm{T}}\boldsymbol{v}_{\mathrm{rel}}^{\mathrm{t}} + C_{\mathrm{R}}\boldsymbol{\omega}_{\mathrm{r}} \times \boldsymbol{n}\right) \tag{9}$$

$$\boldsymbol{\omega}_{\mathrm{r}} = r_i\boldsymbol{\omega}_i + r_j\boldsymbol{\omega}_j \tag{10}$$

where $\boldsymbol{v}_{\mathrm{rel}}$ is the relative translational velocity between particles, $\boldsymbol{n}$ is the unit normal vector, $\boldsymbol{\omega}$ is the particle angular velocity, and the superscripts n and t denote the normal and tangential components, respectively. C_{N}, C_{T} and C_{R} are damping coefficients for the normal, tangential, and rotational movements, respectively, which are functions of liquid viscosity, particle size, inter-particle separation distance, and liquid volume. Washino et al. (2017a, 2017b) proposed viscous force models to evaluate these damping coefficients by approximating the pressure fields inside liquid bridges. **Fig. 23** shows the damping coefficients as a function of inter-particle separation distance obtained from Washino et al. (2017a, 2017b), experiments (Pitois et al., 2000) and Direct Numerical Simulation (DNS), alongside the predictions obtained from other viscous force models in the literature (Adams and Perchard, 1985; Goldman et al., 1967; Pitois et al., 2000). Notably, the results reported by Washino et al., the experiment and DNS exhibit significantly better agreement than those reported by the other models. These models are further extended to apply to both

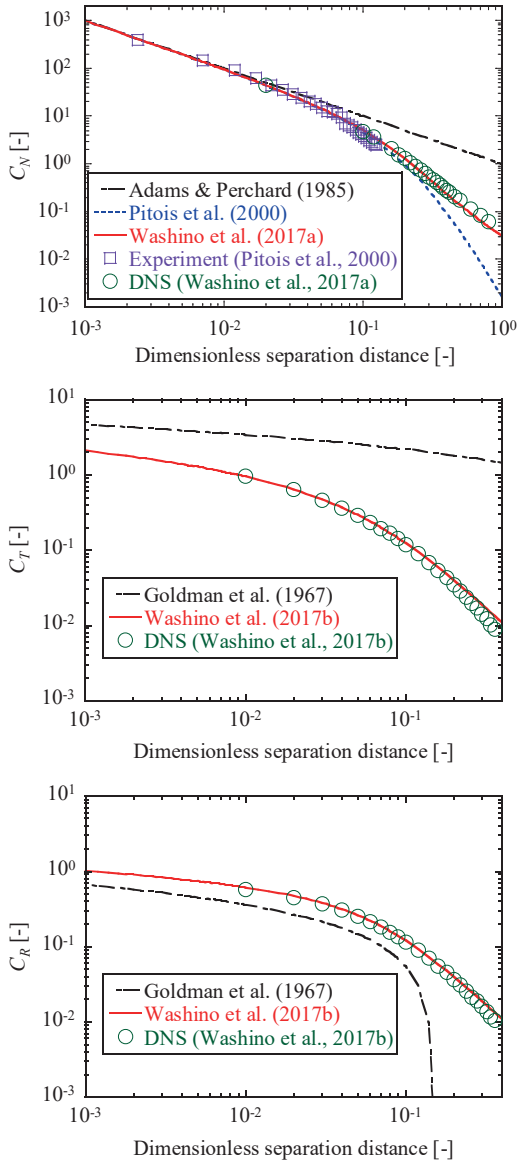

Fig. 23 Comparison between the damping coefficients obtained from Washino et al., experiment, and DNS, along with the predictions obtained from other models in the literature. Reproduced from the work by Washino et al. (Washino et al., 2017a, 2017b).

Newtonian and power-law fluids (Washino et al., 2018b; 2021b).

6.5 Modeling large objects

In applications such as combustion, gasification, and granulation processes, solid particles exhibit significant size variations that often span multiple orders of magnitude. As an extension of the DEM–CFD model, Tsuji et al. (2014) proposed the Fictitious Particle Method (FPM), which combines particle-resolved simulations for large particles with the conventional DEM–CFD for small particles. Inspired by the Volume Penalization Method, FPM estimates the momentum exchange between fluids and solids by representing a large particle as an assembly of small, dense fictitious particles. As demonstrated in **Fig. 24**, this method successfully reproduced the sinking and floating behaviors of large spheres in a bubbling fluidized bed, depending on their density (Higashida et al., 2016a; Tsuji et al., 2014). The model was later extended to large non-spherical particles by incorporating the Super-Ellipsoid (SE) model (Tsuji et al., 2022).

6.6 Heat and mass transfer modeling

Owing to their large gas–solid contact area and efficient particle mixing, fluidized beds are extensively employed in industrial processes in which heat and mass transfer are of primary importance. Sakurai et al. (2009) proposed a DEM–CFD model incorporating heat transfer. Focusing on temperature ranges below 500 K, the proposed model considers only conductive and convective heat transfer, neglecting the influence of radiative heat transfer. The use of a reduced spring constant results in an excessively large contact area, which leads to an overestimation of the conductive heat transfer. To avoid this problem, the contact area was determined by using the actual particle stiffness based on the contact forces obtained with a reduced spring constant. To account for the influence of turbulence, the Smagorinsky model used for the large-eddy simulation was modified to incorporate the effect of the void fraction. The model demonstrated reasonable agreement with experimental results obtained using an infrared thermography camera. Later, the model was extended to mass transfer cases such as particle drying.

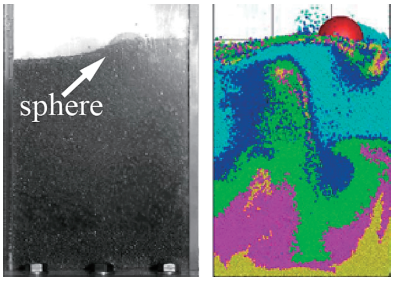

Fig. 24 Floating of a large sphere in a bubbling fluidized bed (Tsuji et al., 2014).

7. Large-scale simulations and applications

7.1 Large-scale DEM–CFD simulation of a three-dimensional fluidized bed

Improvements in computer performance and the development of large-scale computing environments, such as parallel computing, have made it possible to perform large-scale DEM–CFD simulations. When resolving the bubbles that form in fluidized beds, a particle number of approximately 10^4 (100^2) in the case of 2D and 10^6 (100^3) in the case of 3D is required to represent bubbles with a diameter of several dozen grains.

Fig. 25 shows the results of a calculation of a three-dimensional fluidized bed under the condition of 4.5 million particles (Tsuji et al., 2008b). This particle number enables the simulation to capture the complex interactions of multiple bubbles in a three-dimensional fluidized bed.

7.2 Cluster formation induced by large differences in particle size

Fig. 26 shows the simulation results for a fluidized bed containing a binary particle mixture with a large size ratio ($d_{pL}/d_{pS} = 20$). These results were obtained using the FPM described in **Section 6.5**. In the figure, the small particles are color-coded to highlight the motion of the particle phase. In this calculation, the CFD cell size was set to be larger than the small particles but smaller than the large

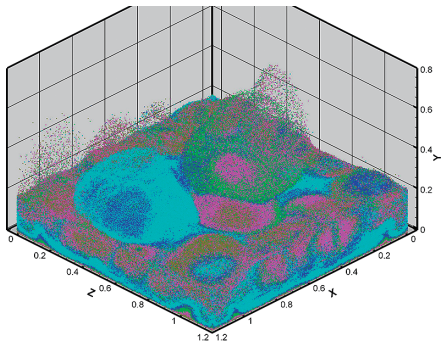

(a) Fluidized behavior

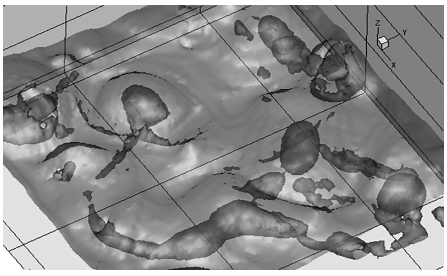

(b) Inner structure of bubbles

Fig. 25 Large-scale DEM–CFD simulation of a three-dimensional fluidized bed. Reprinted from Ref. (Tsuji et al., 2008b). Copyright (2007), with permission from Elsevier.

particles, allowing the fluid flow around the larger particles to be resolved. The simulation successfully captured the formation of particle clusters within bubbles, where small particles were entrained and dragged downward in the wake of large particles descending through the bubbles (Higashida et al., 2016b).

7.3 Mixing and segregation behaviors in vibrated fluidized beds

The addition of mechanical vibration can enhance the mixing and segregation of particles in fluidized beds, although the additional energy input from the vibration increases the complexity. Jiang et al. (2020) developed a DEM–CFD model for vibrated fluidized beds that incorporates the influence of mechanical vibration as well as the aeration. The model was constructed in a non-inertial frame of reference fixed to the vibrating bed, with inertial force terms appearing in the governing equations. Focusing on the density segregation of a binary particle system under a vertical vibration, the model successfully reproduced a sharp transition from reverse segregation (heavy particles on top) to forward segregation (light particles on top) as a function of gas superficial velocity (**Fig. 27**). The numerical results clarified that the transition originates from a directional change in the gas pressure gradient formed within the bed (Jiang et al., 2023).

7.4 Plate penetration into granular materials

For the improved engineering design and operation of construction and mining machinery, as well as off-road robots, it is crucial to understand the interactions between ground granular materials such as clays, sands, gravels, and rocks and mechanical components that directly engage with them (e.g., buckets, blades, legs, belts, and wheels). The response of granular materials is influenced by multiple factors, and the detailed mechanisms governing these interactions remain insufficiently understood.

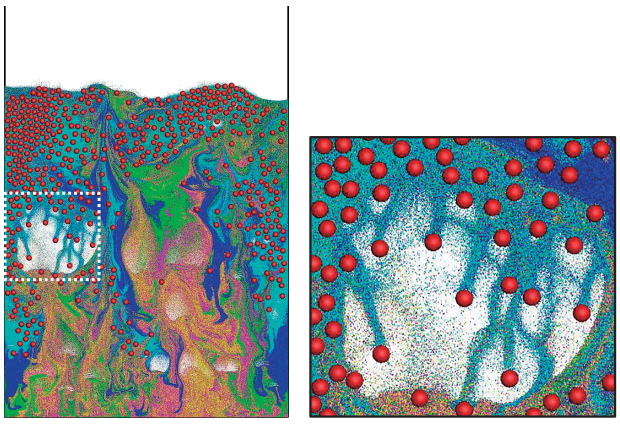

(a) Entire view (b) Magnified view

Fig. 26 Cluster formation induced by large differences in particle size (Higashida et al., 2016b).

Kobayakawa et al. (2018) investigated the influence of the initial packing fraction on plate dragging through large-scale DEM simulations involving more than 33 million particles. Their study demonstrated packing-fraction-dependent bifurcation in the drag force. In an initially loose granular bed, the drag force stabilizes at an approximately constant value as the plate advances, whereas in an initially dense bed, the drag force exhibits large-amplitude oscillations. They attributed this oscillatory behavior to the periodic evolution of a shear band, which formed exclusively in the dense bed (**Fig. 28**). Kobayakawa et al. (2020) examined the influence of the rake angle of a plate in a dense bed. They found that the relationships among the rake angle, evolution of the shear band, and drag force can be quantitatively explained using a three-dimensional wedge model that accounts for variations in the local volume fraction within the shear band.

Miyai et al. (2019) focused on the influence of particle size on the vertical penetration of a flat plate by changing the mean particle diameters d_{50} but maintaining the plate thickness B from $B/d_{50} = 63$ to 2.6. In the smallest particle size case ($B/d_{50} = 63$), the size ratio reached almost the same level as that in the laboratory experiments using

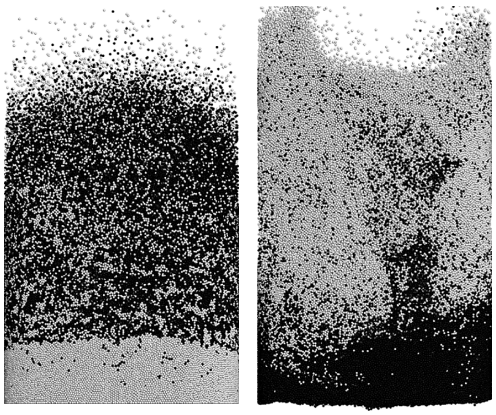

(a) Reverse ($u_0 = 0$ m/s) (b) Forward ($u_0 = 0.181$ m/s)

Fig. 27 Reverse and forward segregation in a vibrated fluidized bed where the density of black and white particles of $\rho_p = 4000$ kg/m^3 and 1500 kg/m^3, respectively (Jiang et al., 2023).

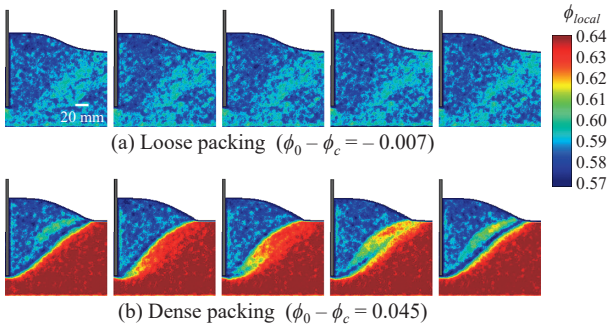

(a) Loose packing ($\phi_0 - \phi_c = -0.007$)

(b) Dense packing ($\phi_0 - \phi_c = 0.045$)

Fig. 28 Dependency of local volume fraction distribution on the initial packing fraction during horizontal dragging. Reprinted from Ref. (Kobayakawa et al., 2020) under the terms of the CC BY 4.0 license.

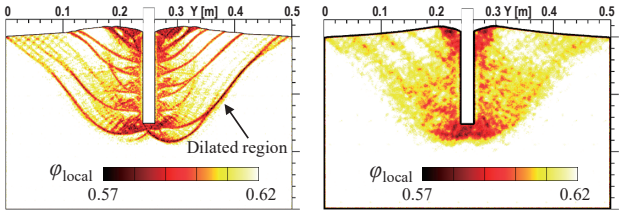

(a) $B/d_{50} = 63$ (b) $B/d_{50} = 21$

Fig. 29 Dependency of local volume fraction distribution on particle size during vertical penetration. Only the results for $B/d_{50} = 63$ and 21 are presented here. Reprinted from Ref. (Miyai et al., 2019) under the terms of the CC BY 4.0 license.

natural sand particles. After careful calibration and model validation, the authors reported qualitative behavioral changes between $B/d_{50} = 31$ and 21. For the large B/d_{50} cases, the resistance exhibited quasi-periodic fluctuations, which were attributable to the intermittent nucleation and disappearance of the shear bands (**Fig. 29**).

7.5 DEM and continuum models

The $\mu(I)$ rheology is one of the most commonly used continuum models for describing dense granular flows. However, as a local model, it cannot capture the influence of microscopic interactions, which are known as grain-size effects, on macroscopic behavior. Nonlocal models, such as the Nonlocal Granular Fluidity (NGF) model, are generally applicable only to dry materials. To address this limitation, Faroux et al. (2022a) investigated the nonlocal rheological characteristics of wet granular materials using DEM, taking capillary forces into account. Applying a coarse-graining procedure, they examined the granular fluidity field predicted by the NGF theory and explored its relationship with material cohesiveness through the Bond number. By limiting the scope to critical-state areas and using normalizations based on the granular temperature, exponential-type cohesive constitutive laws were obtained. Numerical implementations of the NGF model in continuum calculations were also explored (Faroux et al., 2022b, 2022c).

8. Particle-resolved simulations

8.1 Simulation method and coupling technique

The proliferation of computational resources has enabled particle-resolved direct numerical simulations (PR-DNS) nowadays, wherein the microscopic flow around and between particles is captured by directly solving the Navier–Stokes equations. Although computational resources have become more abundant, the computational load of PR-DNS remains substantial, making efficient computation particularly essential. Coupling techniques, such as the Immersed Boundary Method (IBM) with DEM (Fujihara et al., 2013), and the Volume Penalization (VP) method with DEM (Nguyen et al., 2021a), have been developed. These techniques have been employed to investigate problems involving microscopic phenomena that cannot be captured within the framework of particle-unresolved DEM–CFD models.

8.2 Hindered settling

Particle-resolved direct numerical simulations were used to study the hindered settling of monodisperse spheres. Prior to performing the actual simulations for hindered settling, extensive benchmarking studies were conducted for fixed spheres (Zaidi et al., 2014a). A mathematical relationship is proposed for the average drag force, which can be used in mesoscopic simulations.

Subsequently, simulations were performed for hindered settling for Reynolds numbers up to 50 (Zaidi et al., 2015a). It was observed that the average settling velocity obtained by the simulations deviated from the well-known power law proposed by Richardson and Zaki (1997) for low solid volume fractions and moderate Reynolds number. It was found that this was due to two-body hydrodynamic interactions or Drafting-Kissing-Tumbling (DKT) (Fortes et al., 1987). For low solid volume fractions and moderate Reynolds numbers, strong two-body hydrodynamic interactions led to horizontally separated particles (Zaidi et al., 2015b). It is known that horizontally separated particles experience larger drag forces. Thus, the average settling velocity decreased.

In the study of moderate Reynolds number ($1 \leq Re \leq 50$), it was observed that dilute regime showed deviation from the power law proposed by Richardson and Zaki (1997). Thus, the dilute regime was further investigated at higher Reynolds numbers ($Re \leq 300$) (Zaidi et al., 2014b). It was observed that in the higher Reynolds number range ($175 \leq Re \leq 300$), particles form elongated column-like clusters under dilute conditions. This cluster formation increases the average settling velocity and the velocity fluctuations during settling. The increase in the settling velocity is due to the entrapment of particles in strong wakes, where particles experience lower drag; thus, the average settling velocity increases. It was found that the velocity fluctuations of the fluid increased due to vortex shedding from particle clusters, which are not present in the case of moderate Reynolds number ($1 \leq Re \leq 50$).

8.3 Influence of the sidewall

The inhomogeneity of the particle structure in flow is induced by the presence of solid walls, leading to the formation of preferential flows at the particle scale and inhomogeneous fluid forces acting on the particles. Using PR-DNS, Tsuji et al. (2013) investigated the influence of sidewalls parallel to the main flow by varying the bulk void fraction, particle Reynolds number, and particle diameter while keeping all particles fixed in the domain. **Fig. 30** shows the time-averaged void fraction and streamwise flow

velocity distributions as a function of distance from the sidewall x, normalized by the particle diameter d_p. The results correspond to a bulk void fraction of $\varepsilon = 0.503$, whereas the particle Reynolds number was varied. Due to the constraints imposed by the sidewalls and interactions with surrounding particles, the local void fraction exhibits an oscillatory profile at the particle scale. Consequently, the flow velocity profile also becomes oscillatory. By performing spatial averaging on the data obtained from PR-DNS, it is possible to quantitatively assess the predictive performance of empirical drag models used in particle-unresolved DEM–CFD simulations. **Fig. 31** shows that the Ergun (1952) and Beetstra et al. (2007) equations significantly underpredict the pressure drop near the wall ($0 < \Delta x/d_p < 1$), which is attributed to the inhomogeneities at the particle scale.

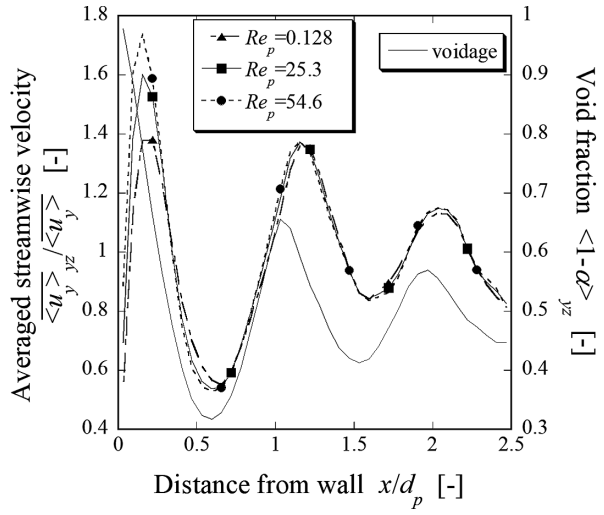

Fig. 30 Time-averaged void fraction and streamwise velocity distributions versus distance from the wall ($\varepsilon = 0.503$). Reprinted from Ref. (Tsuji et al., 2013). Copyright (2013), with permission from Elsevier.

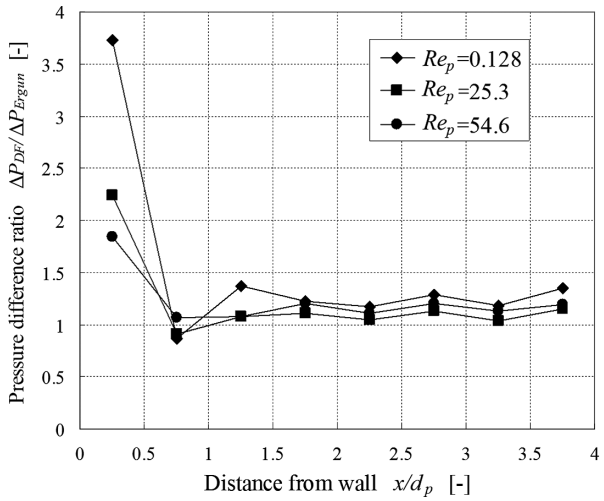

Fig. 31 Assessment of pressure drop predicted by the Ergun equations ($\varepsilon = 0.503$). Reprinted from Ref. (Tsuji et al., 2013). Copyright (2013), with permission from Elsevier.

8.4 Gas–liquid–solid three-phase flow

Gas–liquid–solid three-phase flows can be encountered in many industrial processes, including chemical reactors, slurry mixing, capillary suspensions, and 3D printing. In such processes, gas, liquid, and solid particles coexist in the same system and flow together while interacting. For simulating three-phase flows, the particles are often treated as discrete entities using DEM, whereas the fluids (i.e., both gas and liquid phases) are collectively handled as a continuum with either the interface-tracking method (Tryggvason et al., 2001; Unverdi and Tryggvason, 1992) or interface-capturing method (Hirt and Nichols, 1981; Osher and Sethian, 1988; Takewaki and Yabe, 1987). Recently, the authors developed a three-phase simulation model that can accurately account for the fluid–solid and three-phase interactions.

The fluid–solid interactions are modeled with the Volume Penalization (VP) method with optimal permeability (Nguyen et al., 2021a). **Fig. 32** shows segregations in liquid–solid fluidized beds predicted by the developed model. It is found that these segregations are induced by (a) imbalance between the fluid and gravitational forces due to different densities and (b) differences in fluid forces caused by particle shapes.

For the three-phase interactions, a combination of the Immersed Free Surface (IFS) model (Nguyen et al., 2021b) and the Continuous Capillary Force (CCF) model (Washino et al., 2013) is employed. The IFS model smoothly extends

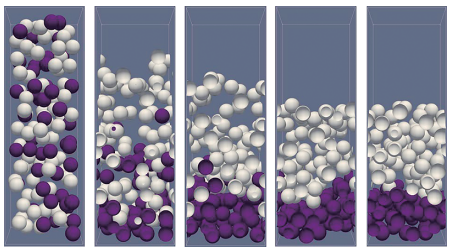

(a) Density segregation

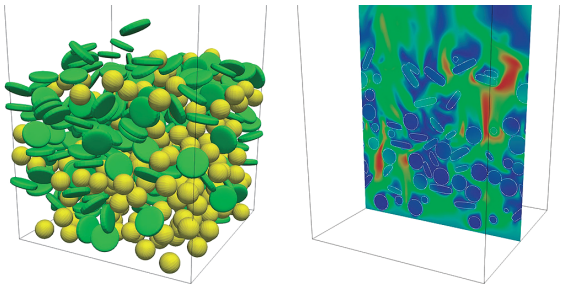

(b) Shape segregation

Fig. 32 Segregations in liquid–solid fluidized beds caused by **(a)** density and **(b)** shape differences. In **(a)**, the density of the purple particles is higher than that of the white particles. In **(b)**, the color map shows the fluid velocity magnitudes, ranging from 0 m/s (blue) to 0.45 m/s (red). **(a)** is reprinted from Ref. (Nguyen et al., 2021a) under the terms of the CC BY-NC-ND 4.0 license, and **(b)** from Ref. (Washino et al., 2023b). Copyright (2023), with permission from Elsevier.

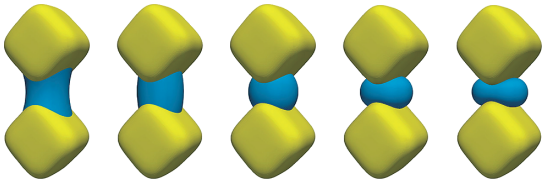

Fig. 33 Snapshots of liquid bridges between two stationary cube-like particles with different contact angles; 30°, 60°, 90°, 120° and 150° from left to right. Reprinted from Ref. (Washino et al., 2023b). Copyright (2023), with permission from Elsevier.

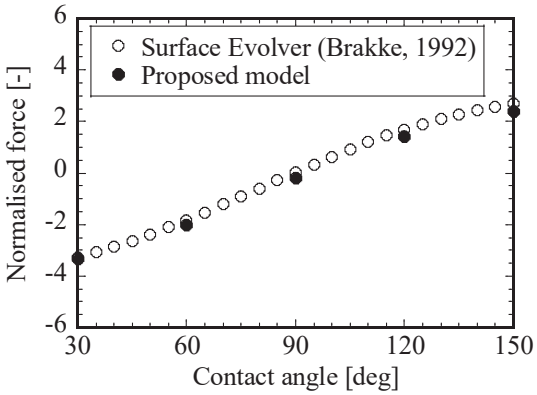

Fig. 34 Normalized capillary forces as a function of contact angle. Reprinted from Ref. (Washino et al., 2023b). Copyright (2023), with permission from Elsevier.

the gas–liquid interfaces from the exterior of the particle to the interior with a specified contact angle, whereas the CCF model converts the surface tension at the three-phase contact line into a body force so that the capillary force can be computed via a volume integral rather than a line integral. It can be seen that the IFS model can account for the solid surface wettability (**Fig. 33**), and the corresponding capillary forces can be well predicted using the CCF models (**Fig. 34**).

The developed model has the potential to simulate complex three-phase flows in various industrial processes. One example of such flows is bubble rise in a liquid mixed with differently shaped particles (**Fig. 35**). It was found in the simulation that the particles take preferential orientations depending on their shapes so that their projection areas to the flow field induced by the rising bubble are minimized.

9. Concluding remarks

The present article provides a brief overview of the authors' studies on discrete particle modeling and simulation of granular, gas–solid, liquid–solid, and gas–liquid–solid flows, where particle–particle interactions cannot be neglected. With the rapid development in computing power and AI technology, it is expected that the development and use of DEM–CFD simulations will continue to advance in the future.

The modeling and development of computational methods for the various complex problems associated with dense gas–solid two-phase flow or high-concentration particle flow, including liquid bridging, particle shape, particle surface properties (including wettability), lubrication, heat transfer, and chemical reactions, remain active areas of research. The authors hope that this review will contribute to the future development of this field.

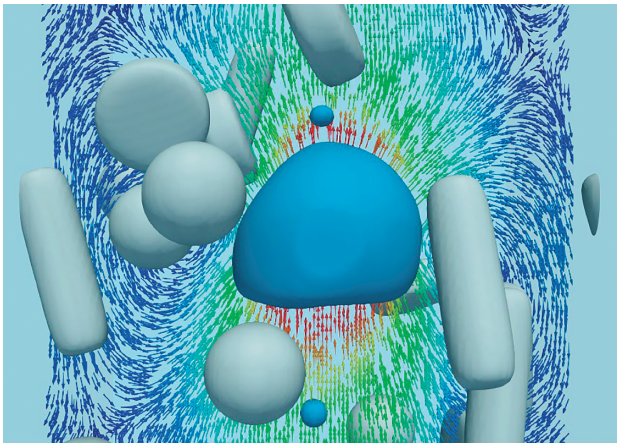

Fig. 35 Bubble rise in liquid mixed with differently shaped particles. The vectors indicate the fluid velocity field at the cross-section. The color map shows the magnitude of the fluid velocity from 0 m/s (blue) to 0.2 m/s (red). Reprinted from Ref. (Washino et al., 2023b). Copyright (2023), with permission from Elsevier.

Nomenclature

CFD	Computational fluid dynamics
DAFM	Dynamic adhesion force model
DEM	Discrete element method
DKT	Drafting–kissing–tumbling
DSMC	Direct simulation Monte Carlo
FPM	Fictitious particle method
PSI Cell	Particle-source-in cell
TFM	Two-fluid model
a	particle radius (m)
B	plate thickness (m)
C_{N}	normal damping coefficient (kg/s)
C_{R}	rotational damping coefficient (kg/s)
C_{T}	tangential damping coefficient (kg/s)
d_{p}	particle diameter (m)
d_{50}	median diameter of particles (m)
d_{pL}	particle diameter of large particle (m)
d_{pS}	particle diameter of small particle (m)
e	restitution coefficient (-)
E	Young's modulus (Pa)
f_{Cn}	elastic repulsive force (N)
F_{AD}	adhesion force (N)
$\boldsymbol{F}_{\mathrm{B}}$	body force (N)
$\boldsymbol{F}_{\mathrm{I}}$	inter-particle force (N)
$\boldsymbol{F}_{\mathrm{vis}}$	viscous force (N)
k	normal spring constant (N/m)
k_{D}	normal spring constant of DAFM (N/m)
k_{R}	normal spring constant without DAFM (N/m)
m	mass (kg)
$\boldsymbol{M}_{\mathrm{I}}$	inter-particle torque (Nm)
$\boldsymbol{n}$	unit normal vector (-)

r	radius (m)
R	pipe radius (m)
St	Stokes number (-)
t	time (s)
Δt	time duration of explosion (s)
v_c	critical collision velocity (m/s)
v_{pz}	particle velocity in vertical direction (m/s)
v'_{pz}	particle fluctuation velocity in vertical direction (m/s)
v_{pt}	particle fluctuation velocity in transverse direction (m/s)
$\boldsymbol{v}_{rel}$	relative velocity (m/s)
α	parameter (-)
$\dot{\gamma}$	shear rate (s^{-1})
δ_n	normal deformation (m)
Δx	mesh size used in CFD calculation (m)
ε	Bulk void fraction (-)
κ_n	constant of normal elastic repulsion (-)
ρ_p	density of particle (kg/m^3)
σ	Poisson's ratio (-)
τ_{yx}	shear stress (Pa)
$\boldsymbol{\omega}$	particle angular velocity (rad/s)

References

Adams M.J., Perchard V., The cohesive forces between particles with interstitial liquid, Institute of Chemical Engineering Symposium, 91 (1985) 147–160.

Anderson T.B., Jackson R., Fluid mechanical description of fluidized beds: equations of motion, Industrial and Engineering Chemistry Fundamentals, 6 (1967) 527–539. https://doi.org/10.1021/i160024a007

Beetstra R., van der Hoef M.A., Kuipers J.A.M., Drag force of intermediate Reynolds number flow past mono- and bidisperse arrays of spheres, AIChE Journal, 53 (2007) 489–501. https://doi.org/10.1002/aic.11065

Bierwisch C., Kraft T., Riedel H., Moseler M., Three-dimensional discrete element models for the granular statics and dynamics of powders in cavity filling, Journal of the Mechanics and Physics of Solids, 57 (2009) 10–31. https://doi.org/10.1016/j.jmps.2008.10.006

Bird G.A., Molecular Gas Dynamics and the Direct Simulation of Gas Flows, 2nd edition, Oxford University Press, 1994, ISBN: 9780198561958. https://doi.org/10.1093/oso/9780198561958.001.0001

Bouillard J.X., Lyczkowski R.W., Gidaspow D., Porosity distributions in a fluidized bed with an immersed obstacle, AIChE Journal, 35 (1989) 908–922. https://doi.org/10.1002/aic.690350604

Chan E.L., Washino K., Coarse grain model for DEM simulation of dense and dynamic particle flow with liquid bridge forces, Chemical Engineering Research and Design, 132 (2018) 1060–1069. https://doi.org/10.1016/j.cherd.2017.12.033

Crowe C.T., Review—numerical models for dilute gas-particle flows, Journal of Fluids Engineering, 104 (1982) 297–303. https://doi.org/10.1115/1.3241835

Crowe C.T., Sharma M.P., Stock D.E., The particle-source-in cell (PSI-CELL) model for gas-droplet flows, Journal of Fluids Engineering, 99 (1977) 325–332. https://doi.org/10.1115/1.3448756

Cundall P.A., Strack O.D.L., A discrete numerical model for granular assemblies, Geotechnique, 29 (1979) 47–65. https://doi.org/10.1680/geot.1979.29.1.47

Ergun S., Fluid flow through packed columns, Chemical Engineering and Processing, 48 (1952) 89–94.

Faroux D., Washino K., Tsuji T., Tanaka T., Granular fluidity in cohesive split-bottom granular flows, Physical Review Fluids, 7 (2022a) 084306. https://doi.org/10.1103/PhysRevFluids.7.084306

Faroux D., Washino K., Tsuji T., Tanaka T., A FVM implementation and validation of non-local modeling for single- and two-phase granular flows, Computational Particle Mechanics, 9 (2022b) 1249–1263. https://doi.org/10.1007/s40571-021-00455-5

Faroux D., Washino K., Tsuji T., Tanaka T., 3D implementation and validation of VOF-coupled non-local granular rheology, Granular Matter, 24 (2022c) 52. https://doi.org/10.1007/s10035-022-01212-y

Fortes A.F., Joseph D.D., Lundgren T.S., Nonlinear mechanics of fluidization of beds of spherical particles, Journal of Fluid Mechanics, 177 (1987) 467–483. https://doi.org/10.1017/S0022112087001046

Fujihara S., Tsuji Takuya, Tanaka T., Effect of a wall on flow with dense particles (a case with moving particles), Japanese Journal of Multiphase Flow, 26 (2013) 489–497. https://doi.org/10.3811/jjmf.26.489

Gera D., Gautam M., Tsuji Y., Kawaguchi T., Tanaka T., Computer simulation of bubbles in large-particle fluidized beds, Powder Technology, 98 (1998) 38–47. https://doi.org/10.1016/S0032-5910(98)00017-5

Goldman A.J., Cox R.G., Brenner H., Slow viscous motion of a sphere parallel to a plane wall-I Motion through a quiescent fluid, Chemical Engineering Science, 22 (1967) 637–651. https://doi.org/10.1016/0009-2509(67)80047-2

Gore R.A., Crowe C.T., Effect of particle size on modulating turbulent intensity, International Journal of Multiphase Flow, 15 (1989) 279–285. https://doi.org/10.1016/0301-9322(89)90076-1

Hetsroni G., Particles-turbulence interaction, International Journal of Multiphase Flow, 15 (1989) 735–746. https://doi.org/10.1016/0301-9322(89)90037-2

Higashida K., Rai K., Yoshimori W., Ikegai T., Tsuji T., Harada S., Oshitani J., Tanaka T., Dynamic vertical forces working on a large object floating in gas-fluidized bed: discrete particle simulation and Lagrangian measurement, Chemical Engineering Science, 151 (2016a) 105–115. https://doi.org/10.1016/j.ces.2016.05.023

Higashida K., Tsuji T., Tanaka T., DEM-CFD simulation for mixing process of binary particles with large size difference in a bubbling fluidized bed, in: Chaouki J., Berruti F., Bi X., Cocco R. (Eds.), Fluidization XV, 2016b, p. 138. https://dc.engconfintl.org/fluidization_xv/138

Hirt C.W., Nichols B.D., Volume of fluid (VOF) method for the dynamics of free boundaries, Journal of Computational Physics, 39 (1981) 201–225. https://doi.org/10.1016/0021-9991(81)90145-5

Hu Y., Chan E.L., Tsuji T., Tanaka T., Washino K., Geometric similarity on interparticle force evaluation for scaled-up DEM particles, Powder Technology, 404 (2022) 117483. https://doi.org/10.1016/j.powtec.2022.117483

Hu Y., Chan E.L., Watanabe J., Takezawa M., Tsuji T., Tanaka T., Washino K., Inter-particle torque scaling in coarse grained DEM with rolling resistance and particle size distributions, Powder Technology, 438 (2024) 119612. https://doi.org/10.1016/j.powtec.2024.119612

Jiang Z., Rai K., Tsuji T., Washino K., Tanaka T., Oshitani J., Upscaled DEM-CFD model for vibrated fluidized bed based on particle-scale similarities, Advanced Powder Technology, 31 (2020) 4598–4618. https://doi.org/10.1016/j.apt.2020.10.009

Jiang Z., Tsuji T., Oshitani J., Washino K., Tanaka T., Reverse to forward density segregation depending on gas inflow velocity in vibrated fluidized beds, Physics of Fluids, 35 (2023). https://doi.org/10.1063/5.0138556

Johnson K.L., Contact Mechanics, Cambridge University Press, 1985, ISBN:9781139171731.https://doi.org/10.1017/CBO9781139171731

Kawaguchi T., Numerical simulation of fluidized bed using discrete element method, Doctoral Dissertation, Osaka University, Suita, 2003. https://hdl.handle.net/11094/44578

Kawaguchi T., Sakamoto M., Tanaka T., Tsuji Y., Quasi-three-dimensional numerical simulation of spouted beds in cylinder, Powder Technology, 109 (2000a) 3–12. https://doi.org/10.1016/S0032-5910(99)00222-3

Kawaguchi T., Tanaka T., Tsuji Y., Numerical simulation of fluidized bed using the discrete element method: the case of spouting bed, Transactions of the Japan Society of Mechanical Engineers Series B, 58 (1992) 2119–2125. https://doi.org/10.1299/kikaib.58.2119

Kawaguchi T., Tanaka T., Tsuji Y., Numerical simulation of two-dimensional fluidized beds using the discrete element method (comparison between the two- and three-dimensional models), Powder Technology, 96 (1998) 129–138. https://doi.org/10.1016/S0032-5910(97)03366-4

Kawaguchi T., Tanaka T., Tsuji Y., Numerical analysis of density wave in dense gas-solid flows in a vertical pipe, Progress of Theoretical Physics Supplement, 138 (2000b) 696–701. https://doi.org/10.1143/ptps.138.696

Kobayakawa M., Miyai S., Tsuji T., Tanaka T., Local dilation and compaction of granular materials induced by plate drag, Physical Review E, 98 (2018) 052907. https://doi.org/10.1103/PhysRevE.98.052907

Kobayakawa M., Miyai S., Tsuji T., Tanaka T., Interaction between dry granular materials and an inclined plate (comparison between large-scale DEM simulation and three-dimensional wedge model), Journal of Terramechanics, 90 (2020) 3–10. https://doi.org/10.1016/j.jterra.2019.08.006

Kobayashi T., Shimada N., Tanaka T., DEM-CFD coupling simulation of fluidized behavior of Geldart's group A particles - A contact force model for expressing adhesion force, in: ASME-JSME-KSME 2011 Joint Fluids Engineering Conference, AJK 2011, 2011, pp. 3163–3169. https://doi.org/10.1115/AJK2011-12011

Kobayashi T., Tanaka T., Shimada N., Kawaguchi T., DEM-CFD analysis of fluidization behavior of Geldart Group A particles using a dynamic adhesion force model, Powder Technology, 248 (2013) 143–152. https://doi.org/10.1016/j.powtec.2013.02.028

Lambert P., Chau A., Delchambre A., Régnier S., Comparison between two capillary forces models, Langmuir, 24 (2008) 3157–3163. https://doi.org/10.1021/la7036444

Mikami T., Kamiya H., Horio M., Numerical simulation of cohesive powder behavior in a fluidized bed, Chemical Engineering Science, 53 (1998) 1927–1940. https://doi.org/10.1016/S0009-2509(97)00325-4

Mindlin R.D., Compliance of elastic bodies in contact, Journal of Applied Mechanics, Transactions ASME, 16 (1949) 259–268. https://doi.org/10.1115/1.4009973

Mindlin R.D., Deresiewicz H., Elastic spheres in contact under varying oblique forces, Journal of Applied Mechanics, 20 (1953) 327–344. https://doi.org/10.1115/1.4010702

Miyai S., Kobayakawa M., Tsuji T., Tanaka T., Influence of particle size on vertical plate penetration into dense cohesionless granular materials (large-scale DEM simulation using real particle size), Granular Matter, 21 (2019) 105. https://doi.org/10.1007/s10035-019-0961-z

Miyoshi A., Kawaguchi T., Tanaka T., Tsuji Y., Numerical analysis of granular convection in two-dimensional pulsating fluidized bed, Progress of Theoretical Physics Supplement, 138 (2000) 734–735. https://doi.org/10.1143/PTPS.138.734

Morikawa Y., Tsuji Y., Tanaka T., Measurements of horizontal air-solid two-phase flow using an optical fiber probe: particle velocity and concentration, Transactions of the Japan Society of Mechanical Engineers Series B, 51 (1985) 2321–2329. https://doi.org/10.1299/kikaib.51.2321

Muguruma Y., Tanaka T., Tsuji Y., Numerical simulation of particulate flow with liquid bridge between particles (simulation of centrifugal tumbling granulator), Powder Technology, 109 (2000) 49–57. https://doi.org/10.1016/S0032-5910(99)00226-0

Nanbu K., Direct simulation scheme derived from the Boltzmann equations. I. Monocomponent gases, Journal of the Physical Society of Japan, 49 (1980) 2042–2049. https://doi.org/10.1143/JPSJ.49.2042

Nguyen G.T., Chan E.L., Tsuji T., Tanaka T., Washino K., Resolved CFD–DEM coupling simulation using Volume Penalisation method, Advanced Powder Technology, 32 (2021a) 225–236. https://doi.org/10.1016/j.apt.2020.12.004

Nguyen G.T., Chan E.L., Tsuji T., Tanaka T., Washino K., Interface control for resolved CFD-DEM with capillary interactions, Advanced Powder Technology, 32 (2021b) 1410–1425. https://doi.org/10.1016/j.apt.2021.03.004

Osher S., Sethian J.A., Fronts propagating with curvature-dependent speed: algorithm based on Hamilton-Jacobi formulation, Journal of Computational Physics, 79 (1988) 12–49. https://doi.org/10.1016/0021-9991(88)90002-2

Pan Y., Tanaka T., Tsuji Y., Large-eddy simulation of particle-laden rotating channel flow, in: American Society of Mechanical Engineers, Fluids Engineering Division (Publication) FED, Vol. 253, 2000, pp. 797–804.

Pan Y., Tanaka T., Tsuji Y., Direct numerical simulation of particle-laden rotating turbulent channel flow, Physics of Fluids, 13 (2001) 2320–2337. https://doi.org/10.1063/1.1383790

Pan Y., Tanaka T., Tsuji Y., Turbulence modulation by dispersed solid particles in rotating channel flows, International Journal of Multiphase Flow, 28 (2002) 527–552. https://doi.org/10.1016/S0301-9322(01)00084-2

Pitois O., Moucheront P., Chateau X., Liquid bridge between two moving spheres: an experimental study of viscosity effects, Journal of Colloid and Interface Science, 231 (2000) 26–31. https://doi.org/10.1006/jcis.2000.7096

Rabinovich Y.I., Esayanur M.S., Moudgil B.M., Capillary forces between two spheres with a fixed volume liquid bridge: Theory and experiment, Langmuir, 21 (2005) 10992–10997. https://doi.org/10.1021/la0517639

Richardson J.F., Zaki W.N., Sedimentation and fluidisation: part I, Chemical Engineering Research and Design, 75 (1997) S82–S100. https://doi.org/10.1016/S0263-8762(97)80006-8

Sakai M., Koshizuka S., Large-scale discrete element modeling in pneumatic conveying, Chemical Engineering Science, 64 (2009) 533–539. https://doi.org/10.1016/J.CES.2008.10.003

Sakai M., Takahashi H., Pain C.C., Latham J.-P., Xiang J., Study on a large-scale discrete element model for fine particles in a fluidized bed, Advanced Powder Technology, 23 (2012) 673–681. https://doi.org/10.1016/j.apt.2011.08.006

Sakurai T., Minami T., Kawaguchi T., Tsuji T., Tanaka T., Tsuji Y., DEM-CFD simulation and thermography measurement of fluidized bed with heat transfer (fluids engineering), Transactions of the Japan Society of Mechanical Engineers Series B, 75 (2009) 1041–1048. https://doi.org/10.1299/kikaib.75.753_1041

Takewaki H., Yabe T., The cubic-interpolated pseudo particle (CIP) method: application to nonlinear and multi-dimensional hyperbolic equations, Journal of Computational Physics, 70 (1987) 355–372. https://doi.org/10.1016/0021-9991(87)90187-2

Tanaka T., Ishida T., Tsuji Y., Direct numerical simulation of granular plug flow in a horizontal pipe: the case of cohesionless particles, Transactions of the Japan Society of Mechanical Engineers Series B, 57 (1991a) 456–463. https://doi.org/10.1299/kikaib.57.456

Tanaka T., Kadono K., Tsuji Y., Numerical simulation of gas-solid two-phase flow in a vertical pipe: on the effect of particle-to-particle collision, Transactions of the Japan Society of Mechanical Engineers Series B, 56 (1990) 3210–3216. https://doi.org/10.1299/kikaib.56.3210

Tanaka T., Kawaguchi T., Tsuji Y., Discrete particle simulation of flow patterns in two-dimensional gas fluidized beds, International Journal of Modern Physics B, 07 (1993) 1889–1898. https://doi.org/10.1142/S0217979293002663

Tanaka T., Kiribayashi K., Tsuji Y., Monte Carlo simulation of gas-solid flow in vertical pipe or channel, in: Matsui G., Searizawa A., Tsuji Y. (Eds.), Proceedings of International Conference on Multiphase Flows, Tsukuba, 1991b, pp. 439–442.

Tanaka T., Takagi Y., Tsuji Y., Morikawa Y., Measurements of gas-solid two-phase flow in a vertical pipe, Transactions of the Japan Society of Mechanical Engineers Series B, 55 (1989) 2302–2309. https://doi.org/10.1299/kikaib.55.2302

Tanaka T., Tanaka S., Washino K., Tsuji T., DEM analysis of cohesive granular shear flow using dynamic adhesion force model – Model validation for contact-dominated regime, Powder Technology, 447 (2024) 120198. https://doi.org/10.1016/j.powtec.2024.120198

Tanaka T., Tsuji Y., Numerical simulation of gas-solid two-phase flow in a vertical pipe: on the effect of inter-particle collision, in: Stock D.E., Tsuji Y., Jurewicz J.T., Reeks M.W., Gautam M. (Eds.), Gas-Solid Flows 1991: 1st ASME-JSME Fluids Engineering Conference, ASME, Portland, 1991, pp. 123–128.

Tanaka T., Yonemura S., Kiribayashi K., Tsuji Y., Cluster formation and particle-induced instability in gas-solid flows predicted by the DSMC method, JSME International Journal, Series B: Fluids and Thermal Engineering, 39 (1996) 239–245. https://doi.org/10.1299/jsmeb.39.239

Tanaka T., Yonemura S., Tsuji Y., Effects of particle properties on the

structure of clusters, in: American Society of Mechanical Engineers, Fluids Engineering Division (Publication) FED, 1995.

Thakur S.C., Ooi J.Y., Ahmadian H., Scaling of discrete element model parameters for cohesionless and cohesive solid, Powder Technology, 293 (2016) 130–137. https://doi.org/10.1016/J.POWTEC.2015.05.051

Tryggvason G., Bunner B., Esmaeeli A., Juric D., Al-Rawahi N., Tauber W., Han J., Nas S., Jan Y.-J., A front-tracking method for the computations of multiphase flow, Journal of Computational Physics, 169 (2001) 708–759. https://doi.org/10.1006/jcph.2001.6726

Tsuji T., Higashida K., Okuyama Y., Tanaka T., Fictitious particle method: a numerical model for flows including dense solids with large size difference, AIChE Journal, 60 (2014) 1606–1620. https://doi.org/10.1002/aic.14355

Tsuji T., Ito A., Tanaka T., Multi-scale structure of clustering particles, Powder Technology, 179 (2008a) 115–125. https://doi.org/10.1016/j.powtec.2007.07.003

Tsuji T., Narita E., Tanaka T., Effect of a wall on flow with dense particles, Advanced Powder Technology, 24 (2013) 565–574. https://doi.org/10.1016/j.apt.2012.11.006

Tsuji T., Sakamoto Y., Harada S., Uemoto K., Oshitani J., Washino K., Tanaka T., Kajiwara H., Matsuoka K., FPM-SE: a numerical model for dense gas–solid flows with large non-spherical object, Chemical Engineering Science, 264 (2022) 118149. https://doi.org/10.1016/j.ces.2022.118149

Tsuji T., Yabumoto K., Tanaka T., Spontaneous structures in three-dimensional bubbling gas-fluidized bed by parallel DEM–CFD coupling simulation, Powder Technology, 184 (2008b) 132–140. https://doi.org/10.1016/j.powtec.2007.11.042

Tsuji Y., Asano R., Fundamental investigation of plug conveying of cohesionless particles in a vertical pipe (pressure drop and friction of a stationary plug), The Canadian Journal of Chemical Engineering, 68 (1990) 758–767. https://doi.org/10.1002/cjce.5450680504

Tsuji Y., Kawaguchi T., Tanaka T., Discrete particle simulation of two-dimensional fluidized bed, Powder Technology, 77 (1993) 79–87. https://doi.org/10.1016/0032-5910(93)85010-7

Tsuji Y., Morikawa Y., Tanaka T., Karimine K., Nishida S., Measurements and simulation of an air-solid two-phase jet (coarse particles), Transactions of the Japan Society of Mechanical Engineers Series B, 53 (1987a) 2331–2339. https://doi.org/10.1299/kikaib.53.2331

Tsuji Y., Morikawa Y., Tanaka T., Nakatsukasa N., Nakatani M., Numerical simulation of gas-solid two-phase flow in a two-dimensional horizontal channel, International Journal of Multiphase Flow, 13 (1987b) 671–684. https://doi.org/10.1016/0301-9322(87)90044-9

Tsuji Y., Tanaka T., Ishida T., Lagrangian numerical simulation of plug flow of cohesionless particles in a horizontal pipe, Powder Technology, 71 (1992) 239–250. https://doi.org/10.1016/0032-5910(92)88030-L

Unverdi S.O., Tryggvason G., A front-tracking method for viscous, incompressible, multi-fluid flows, Journal of Computational Physics, 100 (1992) 25–37. https://doi.org/10.1016/0021-9991(92)90307-K

Washino K., Chan E.L., Kaji T., Matsuno Y., Tanaka T., On large scale CFD–DEM simulation for gas–liquid–solid three-phase flows, Particuology, 59 (2021a) 2–15. https://doi.org/10.1016/j.partic.2020.05.006

Washino K., Chan E.L., Matsumoto T., Hashino S., Tsuji T., Tanaka T., Normal viscous force of pendular liquid bridge between two relatively moving particles, Journal of Colloid and Interface Science, 494 (2017a) 255–265. https://doi.org/10.1016/j.jcis.2017.01.088

Washino K., Chan E.L., Midou H., Tsuji T., Tanaka T., Tangential viscous force models for pendular liquid bridge of Newtonian fluid between moving particles, Chemical Engineering Science, 174 (2017b) 365–373. https://doi.org/10.1016/j.ces.2017.09.028

Washino K., Chan E.L., Miyazaki K., Tsuji T., Tanaka T., Time step criteria in DEM simulation of wet particles in viscosity dominant systems, Powder Technology, 302 (2016) 100–107. https://doi.org/10.1016/j.powtec.2016.08.018

Washino K., Chan E.L., Nishida Y., Tsuji T., Coarse grained DEM simulation of non-spherical and poly-dispersed particles using scaled-up particle (SUP) model, Powder Technology, 426 (2023a) 118676. https://doi.org/10.1016/j.powtec.2023.118676

Washino K., Chan E.L., Tanaka T., DEM with attraction forces using reduced particle stiffness, Powder Technology, 325 (2018a) 202–208. https://doi.org/10.1016/j.powtec.2017.11.024

Washino K., Chan E.L., Tsujimoto T., Tsuji T., Tanaka T., Development of resolved CFD–DEM coupling model for three-phase flows with non-spherical particles, Chemical Engineering Science, 267 (2023b) 118335. https://doi.org/10.1016/j.ces.2022.118335

Washino K., Hashino S., Midou H., Chan E.L., Tsuji T., Tanaka T., Lubrication force model for a pendular liquid bridge of power-law fluid between two particles, Chemical Engineering Research and Design, 132 (2018b) 1030–1036. https://doi.org/10.1016/j.cherd.2017.12.012

Washino K., Midou H., Chan E.L., Tsuji T., Tanaka T., Model development of tangential hydrodynamic force on particles with pendular liquid bridge of power-law fluid, Journal of Non-Newtonian Fluid Mechanics, 298 (2021b) 104676. https://doi.org/10.1016/j.jnnfm.2021.104676

Washino K., Nakae S., Yamagami R., Chan E.L., Tsuji T., Tanaka T., Scaling of attraction force and rolling resistance in DEM with reduced particle stiffness, Chemical Engineering Research and Design, 203 (2024) 501–519. https://doi.org/10.1016/j.cherd.2024.02.006

Washino K., Tan H.S., Hounslow M.J., Salman A.D., A new capillary force model implemented in micro-scale CFD–DEM coupling for wet granulation, Chemical Engineering Science, 93 (2013) 197–205. https://doi.org/10.1016/j.ces.2013.02.006

Wen C.Y., Yu Y.H., Mechanics of fluidization, Chemical Engineering Progress Symposium Series, 62 (1966) 100–111.

Yamamoto Y., Potthoff M., Tanaka T., Kajishima T., Tsuji Y., Large-eddy simulation of turbulent gas-particle flow in a vertical channel: effect of considering inter-particle collisions, Journal of Fluid Mechanics, 442 (2001) 303–334. https://doi.org/10.1017/S0022112001005092

Zaidi A.A., Tsuji T., Tanaka T., A new relation of drag force for high Stokes number monodisperse spheres by direct numerical simulation, Advanced Powder Technology, 25 (2014a) 1860–1871. https://doi.org/10.1016/j.apt.2014.07.019

Zaidi A.A., Tsuji T., Tanaka T., Direct numerical simulation of finite sized particles settling for high Reynolds number and dilute suspension, International Journal of Heat and Fluid Flow, 50 (2014b) 330–341. https://doi.org/10.1016/j.ijheatfluidflow.2014.09.007

Zaidi A.A., Tsuji T., Tanaka T., Direct numerical simulations of inertial settling of non-Brownian particles, Korean Journal of Chemical Engineering, 32 (2015a) 617–628. https://doi.org/10.1007/s11814-014-0241-x

Zaidi A.A., Tsuji T., Tanaka T., Hindered settling velocity & structure formation during particle settling by direct numerical simulation, Procedia Engineering, 102 (2015b) 1656–1666. https://doi.org/10.1016/j.proeng.2015.01.302

Authors' Short Biographies

Prof. Toshitsugu Tanaka is a Professor Emeritus at The University of Osaka and a Professor in the Faculty of Science and Engineering at Otemon Gakuin University in Japan. He received his Ph.D. from The University of Osaka in 1994. From 2018 to 2019, he served as the President of The Japanese Society for Multiphase Flow, and from 2017 to 2019, he served as the Vice President of The Society of Powder Technology, Japan. His research focuses on gas–solid and particulate flows, particularly on discrete particle modeling and simulations. He has made significant contributions to the development of DEM–CFD simulations for dense gas–solid flows.

Prof. Toshihiro Kawaguchi is a Professor at the Faculty of Societal Safety Sciences, Kansai University, Japan. He worked at The University of Osaka, where he conducted research on gas–solid flows and particle flows. His main contribution of this field is the development of DEM–CFD model for dense gas fluidized beds. He has also expanded the research field to crowd flows. His current research interests are safety and efficiency of crowd flows, including crowd accidents, evacuation from buildings or underground malls, optimal arrangements of stairs or exits, and so on.

Dr. Takuya Tsuji is an Associate Professor in the Department of Mechanical Engineering at The University of Osaka, Japan. After receiving his Ph.D. from Kyushu University in 2004, he joined the department as an Assistant Professor. He was promoted to Research Associate Professor in 2009 and Associate Professor in 2012. His research focuses on numerical modeling and physical elucidation of granular materials and multiphase flows. Since 2024, he has served as a Vice President of The Japanese Society for Multiphase Flow. He has also been serving as the Chief Technology Officer (CTO) of DENSE Ltd., a spin-off company founded in 2020.

Dr. Kimiaki Washino is an Associate Professor of Mechanical Engineering at The University of Osaka, Japan, and Chief Information Officer (CIO) of DENSE Ltd. After receiving his Ph.D. from The University of Sheffield, UK, he worked as a Knowledge Transfer Partnerships (KTP) Associate in a collaboration between the university and Procter & Gamble. His primary expertise lies in simulating gas–liquid–solid three-phase flows and cohesive powder dynamics using Discrete Element Method (DEM) and Computational Fluid Dynamics (CFD). He also serves as an Editor for the journal "Advanced Powder Technology".